







Robust Path Planning via Learning From Demonstrations for Robotic Catheters in Deformable Environments

Zhen Li , Chiara Lambranzi, Di Wu , *Member, IEEE*, Alice Segato , Federico De Marco, Emmanuel Vander Poorten , *Member, IEEE*, Jenny Dankelman , *Member, IEEE*, and Elena De Momi , *Senior Member, IEEE*

Abstract—Objective: Navigation through tortuous and deformable vessels using catheters with limited steering capability underscores the need for reliable path planning. State-of-the-art path planners do not fully account for the deformable nature of the environment. **Methods:** This work proposes a robust path planner via a learning from demonstrations method, named Curriculum Generative Adversarial Imitation Learning (C-GAIL). This path planning framework takes into account the interaction between steerable catheters and vessel walls and the deformable property of vessels. **Results:** *In-silico* comparative experiments show that the proposed network achieves a 38% higher success rate in static environments and 17% higher in dynamic environments compared to a state-of-the-art approach based on GAIL. *In-vitro* validation experiments indicate that the path generated by the proposed C-GAIL path planner achieves a targeting error of 1.26 ± 0.55 mm and a tracking error of 5.18 ± 3.48 mm. These results represent improvements of 41% and 40% over the conventional centerline-following technique for targeting error and tracking error, respectively. **Conclusion:** The proposed C-GAIL path planner

outperforms the state-of-the-art GAIL approach. The *in-vitro* validation experiments demonstrate that the path generated by the proposed C-GAIL path planner aligns better with the actual steering capability of the pneumatic artificial muscle-driven catheter utilized in this study. Therefore, the proposed approach can provide enhanced support to the user in navigating the catheter towards the target with greater accuracy, effectively meeting clinical accuracy requirements. **Significance:** The proposed path planning framework exhibits superior performance in managing uncertainty associated with vessel deformation, thereby resulting in lower tracking errors.

Index Terms—Deep learning, endovascular intervention, path planning, steerable catheter, vessel deformation.

I. INTRODUCTION

ENDOVASCULAR procedures are a rapidly emerging field in medicine. The number of patients treated has constantly increased over the past few decades [1]. These procedures increase patient comfort, reduce risks, and improve outcomes compared to traditional open surgery. However, navigation through narrow, fragile, and deformable vessels, using traditional non-steerable catheters and guidewires, requires considerable skill and experience [2]. Steerable catheters and navigation guidance could potentially lower the skill that would be required for percutaneous treatment [3]. Commercial robotic platforms can attest to the robot-assisted trend, such as CorPathTM GRX (Corindus, Waltham, USA), SenseiTM X and Magellan (J&J robotics, New Brunswick, USA), AmigoTM (Catheter Robotics Inc. Budd Lake, USA), R-OneTM (Robocath, Rouen, France) and NiobeTM (Stereotaxis, St. Louis, USA). In the last decades, different research groups have focused their efforts on the development of steerable catheters [4], [5], [6], [7]. For example, a proof-of-concept medical robotic platform, composed of a multi-lumen catheter shaft and magnetically actuated microcatheter, was developed in [7].

In this study, we explore the application of a novel robotic catheterization system, as detailed in [7], [8], in the context of Percutaneous Coronary Intervention (PCI) for Chronic Total Occlusion (CTO) treatment. This system employs a robotic catheter, innovatively designed with one to two internal lumens. These lumens serve the critical function of carrying microcatheters with magnetic steering capabilities. A key operational

Manuscript received 18 February 2024; revised 30 June 2024; accepted 23 August 2024. Date of publication 29 August 2024; date of current version 16 January 2025. This work was supported by ATLAS project. This project has received funding from the European Union's Horizon 2020 research and innovation programme under the Marie Skłodowska-Curie under Grant Agreement 813782. (*Corresponding author: Elena De Momi.*)

Zhen Li is with the Department of Electronics, Information and Bioengineering, Politecnico di Milano, Italy, and also with the Department of Biomechanical Engineering, Delft University of Technology, The Netherlands.

Chiara Lambranzi is with the Department of Electronics, Information and Bioengineering, Politecnico di Milano, Italy, and also with the Istituto Italiano di Tecnologia, Italy.

Di Wu is with the Department of Mechanical Engineering, Katholieke Universiteit Leuven, Belgium, and also with the Department of Biomechanical Engineering, Delft University of Technology, The Netherlands.

Alice Segato was with the Department of Electronics, Information and Bioengineering, Politecnico di Milano, Italy. He is now with the Nanoflex Robotics, Switzerland.

Federico De Marco is with the Centro Cardiologico Monzino, IRCCS, Italy.

Emmanuel Vander Poorten is with the Department of Mechanical Engineering, Katholieke Universiteit Leuven, Belgium.

Jenny Dankelman is with the Department of Biomechanical Engineering, Delft University of Technology, The Netherlands.

Elena De Momi is with the Department of Electronics, Information and Bioengineering, Politecnico di Milano, 20133 Milan, Italy (e-mail: elena.demomi@polimi.it).

Digital Object Identifier 10.1109/TBME.2024.3452034

TABLE I
STATE-OF-THE-ART PATH PLANNING METHODS FOR ENDOVASCULAR CATHETERIZATION (FROM 2011 TO 2022)

Reference	Method	Algorithm	Instrument	Environment	Validation
[12] Wang 2011	NB	Centerline-based tree	Shaped catheter	Rigid	<i>in-vitro</i>
[13] Zheng 2018	NB	Centerline-based tree	- (Not specified)	Deformable	<i>in-vitro</i>
[14] Huang 2011	NB	Depth first search	Guidewire	Rigid	<i>in-silico</i>
[15] Qian 2019, [16] Cho 2021, [17] Schegg 2022	NB	Dijkstra	Guidewire	Rigid	<i>in-vitro</i>
[18], [19] Ravigopal 2022	NB	Modified hybrid A*	Steerable guidewire	Deformable	<i>ex-vivo</i>
[20] Fagogenis 2019	NB	Wall-following	Concentric tube robot	Deformable	<i>in-vivo</i>
[21], [22], [23] Fauser 2019	SB	bi-RRT	Catheter / Steerable guidewire	Rigid	<i>in-silico</i>
[24] Guo 2021	SB	RRT	Catheter	Rigid	<i>in-silico</i>
[25] Gao 2015	OB	Ant colony optimization	Catheter	Rigid	<i>in-silico</i>
[26] Qi 2019	OB	Optimal inverse kinematics	Steerable catheter	Rigid	<i>in-vitro</i>
[27] Li 2021	OB	Genetic algorithm	Steerable catheter	Rigid	<i>in-silico</i>
[28], [29] Rafii-Tari 2014	LB	GMM, HMM	Shaped catheter, pre-loaded guidewire	Rigid	<i>in-vitro</i>
[30], [31], [10] Chi 2020	LB	DMPs, GMMs, GAIL	Shaped catheter, pre-loaded guidewire	Deformable	<i>in-vitro</i>
[32] Zhao 2022	LB	Generative adversarial network	Guidewire	Rigid	<i>in-vitro</i>
[33] Tibebe 2014, [34] You 2019	LB	Q-learning, deep Q-learning	Steerable catheter	Rigid	<i>in-vitro</i>
[35] Behr 2019, [36] Karstensen 2020, [37] Kweon 2021	LB	deep Q-learning, DDPG	Shaped guidewire	Rigid	<i>in-vitro</i>
[38] Meng 2021	LB	Asynchronous advantage actor-critic	Guidewire	Rigid	<i>in-silico</i>
[39] Karstensen 2022	LB	DDPG	Shaped guidewire	Deformable	<i>ex-vivo</i>
Proposed	LB	C-GAIL	Steerable catheter	Deformable	<i>in-vitro</i>

Acronyms: NB, Node-Based; SB, Sampling-Based; OB, Optimization-Based; LB, Learning-Based; RRT, Rapidly-exploring Random Tree; GMM, Gaussian Mixture Model; HMM, Hidden Markov Model; DMP, Dynamical Movement Primitive; GAIL, Generative Adversarial Imitation Learning; DDPG, Deep Deterministic Policy Gradients.

aspect of this system involves the precise navigation of the robotic catheter to an anchor position proximal to the aortic root. Upon reaching this location, the magnetic microcatheters are subsequently deployed into the coronary arteries, setting the stage for the ensuing treatment procedures. The primary objective of this research is to develop a safe, accurate, and robust path planner for the robotic catheter. This path planner is essential for ensuring the robotic catheter's efficient navigation to the aforementioned anchor position near the aortic root. Limited steering capability underscores the need for reliable path planning [9]. However, the complex interaction between the steerable catheter and vessel walls and the deformable property of the vessels makes reliable and real-time path planning a hard problem.

This work presents a robust and accurate path planning framework to improve risk management. Specifically, this framework can reduce the uncertainty in vessel deformation, thereby minimizing tracking errors. The main contributions are:

- proposing a novel path planning approach, named Curriculum Generative Adversarial Imitation Learning (C-GAIL), which outperforms existing models by offering optimal path planning while adhering to the constraints of robotic catheters. Notably, the C-GAIL integrates a Curriculum Learning (CL) module and a Behavioral Cloning (BC) module, distinguishing it from models like Proximal Policy Optimization (PPO) + Generative Adversarial Imitation Learning (GAIL) ([10], [11]), by enabling progressive training in complex environments from demonstrations;
- presenting a path planning framework for a motorized steerable catheter, which uniquely considers both the deformable nature of the environment and the dynamic movements of the target, setting it apart from existing path planning methods;
- validating the proposed path planner for a motorized steerable catheter in an *in-vitro* setting using a teleoperation control strategy. These experiments underscore the algorithm's feasibility in generating suitable paths that align with the actual steering capability of the catheter, further demonstrating the advantages of the C-GAIL model over a traditional centerline-following approach.

II. RELATED WORK

Over the last decade, several path planning methods for steerable/non-steerable catheters/guidewires have been proposed to assist clinicians. Table I summarizes the state-of-the-art from 2011 to 2022, in terms of path planning methodology, type of medical instrument used, type of environment (presence of dynamic changes), and type of validation (*in-silico*, *in-vitro*, *ex-vivo*, *in-vivo*). In the following a very brief description of the main types of planners is given. For a more detailed literature review, please refer to [40], [41].

A. Node-Based (NB) Methods

Node-based algorithms use an information structure to represent the environment map. Studies [12] and [13] extracted the vessel centerline and built an exploration tree along the centerline. The aim of this method is to keep the tip of the instrument away from the walls. Nevertheless, path exploration inside the information structure is not mentioned in those studies. Graph search strategies such as Depth First Search (DFS) algorithm [14], Dijkstra algorithm [15], [16], [17] and A* algorithm [18], [19] were employed to generate a path solution in a tubular environment with multi-branches. For movement in the cardiac chamber, a wall-following strategy employing haptic vision was developed in [20] by Fagogenis et al. to keep a certain distance from the heart wall.

B. Sampling-Based (SB) Methods

Sampling-based methods randomly sample in the robot's configuration space or workspace to generate new tree vertices. Then collision-free vertices are connected as tree edges. Fauser et al. [21], [22], [23] introduced a bi-directional Rapidly-exploring Random Tree (bi-RRT) method for instruments that follow curvature constrained trajectories in vena cava or aorta. The study in [24] implemented an improved RRT algorithm for cerebrovascular interventions. The expansion direction of the random tree is a compromise between the new randomly sampled node and the target. This strategy can improve the convergence speed of the algorithm. However, their work did not

take into account any kinematic constraints governing catheter movement.

C. Optimization-Based (OB) Methods

Path planning can be formulated as an optimization problem and solved by numerical solvers. Gao et al. [25] proposed an improved Ant Colony Optimization (ACO) algorithm to plan an optimal path that also accounted for factors such as catheter diameter, vascular length, diameter, curvature and torsion. Nevertheless, the high computational time with an average value of 12.32 s makes it infeasible in real-time scenarios. Qi et al. [26] formulated the path planning as an optimization problem under the inverse kinematics modeling of continuum robots. However, the optimization problem is solved locally without considering long-term cumulative costs. Li et al. [27] proposed a fast path planning approach via a local Genetic Algorithm (GA) optimization. The approach is able to account for constraints on the catheter curvature, but the optimization algorithm is based on vessel centerlines that are sensitive to deformations of the anatomical model.

D. Learning-Based (LB) Methods

Learning-based methods use statistical tools and machine learning algorithms for path planning. Rafii-Tari et al. [28], [29] and Chi et al. [10], [30], [31] proposed Learning from Demonstrations (LfD) approaches to optimize trajectories or learn motion primitives using expert demonstrations. Zhao et al. proposed a Generative Adversarial Network (GAN) framework for real-time path planning and evaluated it in 2D-DSA images [32]. The work in [33], [34], [35], [36], [37], [38], [39] developed Reinforcement Learning (RL) approaches to predict a sequence of actions to reach a target. LfD methods based on GAIL were adapted into other medical scenarios [11], [42] because of their ability to compromise between learning the distribution and ensuring the generalization of trajectories. In comparison with the PPO + GAIL model employed in neurosurgery as described in [11], our developed C-GAIL network incorporates additional enhancements through the inclusion of both the BC and CL modules. Moreover, the deformation dynamics in our endovascular intervention setting markedly diverge from those in neurosurgery. Specifically, deformation in our context is induced not solely by the catheter's interaction with the vessel walls but also by the periodic motion associated with the heartbeat. Conversely, neurosurgical procedures typically involve a curvilinear needle trajectory, a simpler navigational challenge than the complex, long, and tortuous routes encountered in blood vessel navigation. These distinctions underscore the specialized challenges of path planning within endovascular interventions relative to neurosurgical applications.

E. Limitations

Current approaches lack planning capabilities that actually take into account the deformable nature of the environment, even while those studies were verified in a soft environment [10], [13], [19], [20], [30], [31], [39]. Moreover, most of the studies

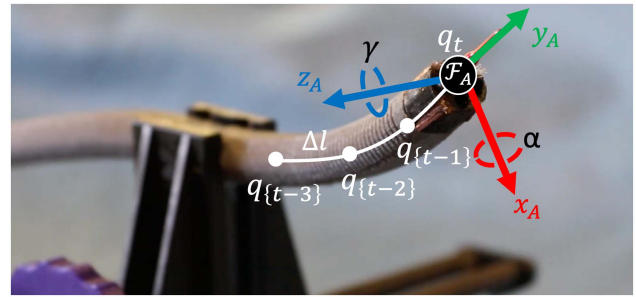


Fig. 1. Parameterization of a robotic catheter agent: The catheter tip has configuration q_t at time t . The agent can perform an insertion movement Δ_l along the y_A axis and can bend with angle α about the x_A axis and with angle γ about the z_A axis, respectively, in the tip frame \mathcal{F}_A . The catheter segments following the tip adopt the previous configurations sequentially.

that looked at deformable environments were actually developed for passive, non-steerable instruments [10], [13], [30], [31], [39]. The wall-following algorithm [20] was only tested on a short path along the inner heart-wall. This approach could be considered efficient if there are few feasible routes to reach the target. However, in scenarios where there are multiple feasible routes, the solution provided by a wall-following algorithm cannot ensure optimality and may cause the catheter to enter other branches along the vessel wall. This algorithm has limited application scenarios. For navigation along vessels, wall-following is not advisable as it could cause the catheter to come into excessive contact with fragile tissue, plaque or calcium that should actually be avoided.

In summary, there is a need for a reliable path planner elaborated in this work that takes into account the deformable nature of the environment and the kinematics of steerable catheters. The paper is built up as follows. Section III introduces the modeling and path planning methods. Section IV presents an *in-silico* and *in-vitro* experimental setup, followed by experimental results in Section V. Conclusions and future directions are summarized in Section VI.

III. MATERIALS AND METHODS

A. Moving Agent

The tip of the catheter is considered as the moving agent. The movement of the catheter is fully determined by the tip under the assumption of Follow-The-Leader (FTL) deployment [3]. While this assumption may not seem very realistic for a catheter with a single bendable segment, it will be shown that it leads to reasonable results.

A fixed coordinate frame \mathcal{F}_A is attached to the tip of the catheter as shown in Fig. 1. The agent can perform an insertion movement Δ_l along the y_A axis and can bend with angle α about the x_A axis and with angle γ about the z_A axis, respectively. The pose of the agent is determined and updated at each time step by the 3-dimensional continuous action space $\mathcal{A} = [\alpha, \gamma, \Delta_l]$. The pose is defined by the tip's position $\mathbf{p}_t = [x, y, z]$ and orientation $\mathbf{r}_t = [\alpha, 0, \gamma]$ in a global frame \mathcal{F}_0 . Using a transformation matrix, the agent configuration q_t can be defined by its pose

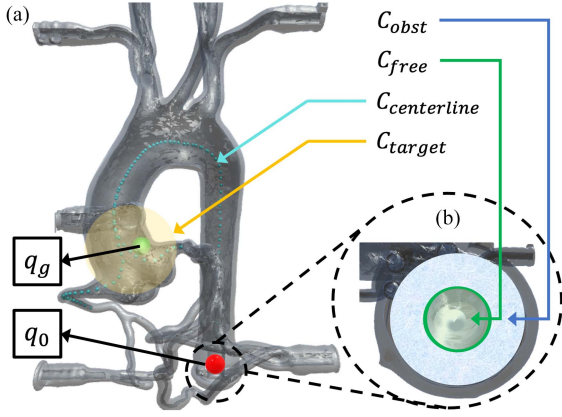


Fig. 2. The environment is represented by an aortic anatomy, the obstacle space C_{obst} , the free space C_{free} , the centerline space $C_{centerline}$, and the target space C_{target} . The catheter moves from the start configuration q_0 and proceeds to move to reach the target configuration q_g . (a) Top view on the aortic model. (b) Cross-sectional view of the open lumen of the descending aorta.

as below, where the superscript T means transpose.

$$q_t = \begin{bmatrix} \mathbf{R}(\alpha, 0, \gamma) & [x, y, z]^T \\ \mathbf{0}^T & 1 \end{bmatrix} \quad (1)$$

The geometric constraints of the catheter, such as its outer diameter and the length of the distal segment L , along with the kinematic constraints, such as the maximum bending angle θ_{\max} and the maximum insertion speed, are considered in the agent's motion. θ_{\max}^t is the maximum bending angle the catheter can bend at time t , given an insertion Δ_l . The bending angle is within the range of $[-\theta_{\max}^t, \theta_{\max}^t]$. This range further depends on the insertion speed v_t and time interval Δ_t because $\Delta_l = v_t \Delta_t$.

$$\theta_{\max}^t = \frac{\theta_{\max} \Delta_l}{L} \quad (2)$$

B. Dynamic Environment

An effective planner should address the level of uncertainty that is present in this problem. Due to the deformable nature of vessels, pre-planned paths will deviate from the reality. Rigidly following such outdated paths may lead to intense contact with the fragile anatomy. A realistic and auto-adaptive simulator to predict vessels' global deformation induced by the catheter's contact and cyclic heartbeat motion was proposed in our previous work [43], [44]. The vessel modeling is based on a Position-based Dynamics (PBD) approach. It discretizes an object into a particle system composed of particles. Then it computes the system's time evolution by directly updating particle positions, subject to a set of equality and inequality constraints. In the developed simulator [43], the deformable property was calibrated according to a stress-strain curve which appropriately depicts the biomechanics properties. Moreover, the heartbeat motion was calibrated according to the averaged annulus displacement from 60 patients with aortic stenosis.

In this work, for the construction of the 3D dynamic environment (see Fig. 2), let us define:

- the “configuration space” C_{space} as the set of all the possible agent configurations q_t ;
- the “obstacle space” $C_{obst} \subset C_{space}$ that is the space occupied by the vessel wall that limits the area in which the catheter can move;
- the “free space” $C_{free} \subset C_{space}$ that is the set of all possible agent configurations q_t within the aorta lumen without collisions with other objects;
- the “centerline space” $C_{centerline}$ that is the shortest path computed via the Voronoi Diagram from the descending aorta to the left and right coronaries;
- the “target space” $C_{target} \subset C_{space}$ that is the volume where the target configuration q_g can locate. Once the delivery catheter reaches the target space, a micro-catheter can be inserted from a channel of the delivery catheter [7]. q_g changes randomly at every learning episode within C_{target} . Importantly, the target moves in concert with the deformation of the vessels, which is induced by the catheter's contact and the cyclic motion of the heartbeat. This movement is achieved by linking the target with one of the particles within the PBD system;
- the agent start configuration q_0 that is located in the descending aorta.

C. Path Planning

The path planning problem can be described as: the agent has to find an admissible set of configurations $Q_t = \{q_0, \dots, q_g\}$ to move from a start position $p_0 \in q_0$ to a target position $p_g \in q_g$. The target position is reached when the distance between the agent and the target is smaller than a distance threshold ϵ .

The state of the agent consists of its pose, that can be changed through the actions of rotation and insertion $\mathcal{A} = [\alpha, \gamma, \Delta_l]$. In training, the agent learns to maximize the reward function by taking actions according to its policy τ , expressed in the paragraph *Reward Function* and by observing its interaction with the environment, described in the subsequent paragraph *Observations*.

1) Reward Function: The reward function $R(\tau) = r_t$ associated with each time step t is designed to optimize the path according to a combination of multiple criteria: the number of steps, the number of collisions, reaching the target position, passing through the centerline waypoints, bending angle. The reward r_t consists of two main parts: r_{end} , a reward added at the end of a learning episode; r_{in} , a relatively small reward added at each step during a learning episode. The reward r_t is expressed in (3)–(5).

$$r_t = r_{end} + r_{in} \quad (3)$$

$$r_{end} = \begin{cases} r_{obst} & \text{if } q_t \in C_{obst} \\ r_{exit} & \text{if } q_t \notin C_{free} \text{ and } q_t \notin C_{obst} \\ r_{target} & \text{if } \|p_t - p_g\| < \epsilon \end{cases} \quad (4)$$

$$r_{in} = r_{step} + r_{centerline} + r_{bending} \quad (5)$$

- r_{obst} is a negative reward that is given if a collision between the catheter tip and vessel walls is detected. We only

TABLE II
VALUES OF THE REWARD FUNCTION PARAMETERS

Reward	Value	Reward	Value
r_{obst}	-1	r_{step}	-1e-5
r_{exit}	-1	$r_{centerline}$	+0.05
r_{target}	+1	$r_{bending}$	+1e-5

take that collision into account because it has a higher risk during navigation. An episode terminates when a non-minor collision occurs;

- r_{exit} is a negative reward when the agent tries to exit from the open lumen down the descending aorta;
- r_{target} is a positive reward given to the agent when it reaches the target;
- r_{step} is a negative reward given at each time step. It is set to keep the total number of steps of the trajectory as small as possible;
- $r_{centerline}$ is a positive reward if the agent reaches a waypoint in $C_{centerline}$;
- $r_{bending}$ is a positive reward that is given when the bending action is bigger than a threshold. This reward was introduced to overcome the tendency of the network to avoid producing actions near the catheter's maximum bending angle. To pass tortuous areas, the maximal bending range is often needed to be able to pass.

The values of the reward function parameters obtained with an empirical method are summarized in Table II. All rewards are set within the interval of [-1, 1]. The minimum value of “-1” is assigned to prohibited behaviors such as violent collisions with the vessel walls. The maximum value of “1” is assigned to reaching the target, which is the agent's task. The other rewards are chosen based on their frequency. For instance, since r_{step} occurs very often, if it is not small enough, it can lead to a large cumulative reward. Similarly, the bending reward also has the potential to lead to a large cumulative reward. In contrast, the number of centerline points is relatively small, with only around 100 points, and not all of them are reachable if the catheter constraints are met. Hence, this positive reward is set slightly larger.

2) Observations: At every step, the agent collects observations o_t , which are composed of:

- the agent configuration q_t ;
- the normalized distance from the agent to the target $u = \frac{\|p_g - p_t\|}{d_{max}}$, where d_{max} is the maximum distance between the agent and the target when $q_t \in C_{free}$;
- the direction from the agent to the target $v = p_g - p_t$;
- a set of raycast observations o_{ray} . Each raycast detects the presence of the aortic wall along its direction within the ray length.

3) C-GAIL Network: The new network proposed in this paper, named C-GAIL network, is built around the combination of the principles of LfD and RL (see Fig. 3). The LfD component is realized through BC and GAIL networks. The PPO network has two parts: the actor network provides an action given the observation; the critic network that evaluates the actor network using the extrinsic reward and suggests modification according

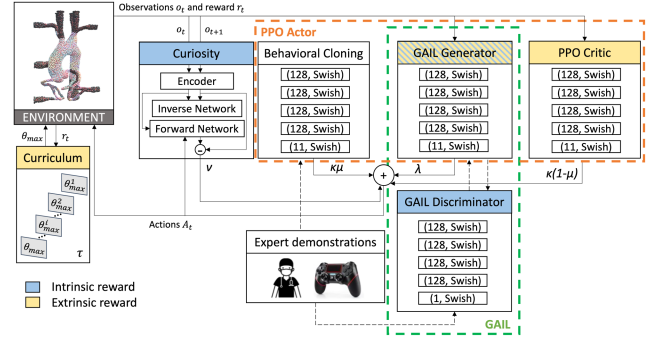


Fig. 3. The proposed C-GAIL network architecture. The extrinsic reward signal considers the reward given by interacting with the environment, such as curriculum and PPO modules. The intrinsic reward has a policy that considers other factors, and it is defined inside the learning algorithm: for GAIL about the similarity of the path with respect to the expert demonstrations, for curiosity about the difference between the predicted and the actual path.

to a gradient ascent policy. The actor network updates its actions according to three policies: the BC policy, PPO policy, and the GAIL generator policy. The curiosity module [45] acts as an intrinsic reward signal that enables the agent to explore its environment in novel states to help escape local minima of the policy function. The curiosity module contains an inverse and forward network. The inverse network predicts the action between observations, while the forward network predicts the next encoded observation. The difference between the predicted and actual encoded observations is defined as the loss of the forward network. Therefore, through curiosity-driven exploration, the agent can predict the outcome of its actions and acquire skills that may be valuable in the future. The curriculum learning module acts on the environment by progressively adding complexity during the training [46]. The curriculum learning module optimizes the bending angle while respecting the reachable bending range of the catheter. Specifically, in curriculum learning, the learning progress is measured through the reward function and once the agent performance improves, θ_{max} is decreased for the next level of learning. Finally, the agent is able to try actions in different reachable bending ranges and obtain globally optimal paths.

The proposed network can be represented as a set of modules with weights, that define the contribution of each module to the loss function. These modules interact with the environment and with each other. The goal is to come up with an optimal combination of the strengths of the different modules such that a performance is achieved that exceeds those of the offered demonstrations. The training is based on the linear combination of the respective RL and LfD losses:

$$\mathcal{L} = \kappa(1 - \mu)\mathcal{L}_{PPO} + \lambda\mathcal{L}_{GAIL} + \kappa\mu\mathcal{L}_{BC} + \nu\mathcal{L}_{curiosity} \quad (6)$$

where \mathcal{L}_{PPO} is the PPO critic network loss (see its definition in [47]), \mathcal{L}_{GAIL} is the GAIL loss [48], \mathcal{L}_{BC} is the BC loss [49], $\mathcal{L}_{curiosity}$ is the curiosity loss [45]. The weight μ indicates the degree to which we prioritize the influence of BC over the policy relative to PPO, with a higher weight indicating a higher learning

rate of imitation from demonstrations and a lower weight indicating more operations attempting to maximize reward rather than imitating. The following weights were found empirically to work well: $\kappa = 0.2$, $\lambda = 0.8$, $\mu = 0.7$, $\nu = 0.02$. The GAIL is given the highest weight because the method combines two paradigms and reward types, intrinsic and extrinsic. The selection process for these weights involved a systematic evaluation. Initially, a wide array of weight combinations underwent testing in preliminary trials to pinpoint those substantially impacting model performance. This was followed by narrowing our focus to specific ranges surrounding these effective values. The definitive weights were selected based on their consistent contribution to enhanced performance metrics, detailed in Section IV-C.

D. Clinical Workflow for the Proposed Path Planner

Regarding the clinical translation of this work, the anticipated clinical workflow is designed as follows.

- Firstly, a 3D mesh model is reconstructed from the pre-operative Computed Tomography Angiography (CTA) images of a specific patient using the *AW server* (GE Healthcare). Based on this 3D model, a patient-specific deformable environment is built using the PBD simulator [43]. In this simulator, Particle Swarm Optimization (PSO) is employed to derive the optimal PBD parameters that accurately replicate the stress-strain curve of blood vessels and to simulate the vessels' movements resulting from heartbeat. The calibration of heartbeat movements is based on the average annulus displacement derived from 60 patients with aortic stenosis. Furthermore, should data on the specific properties of a patient's blood vessels be available, the simulator can be tailored to reflect patient-specific characteristics.
- Then, the proposed C-GAIL network undergoes training with expert-provided, patient-specific demonstrations, which may encompass approximately 70 instances. This model can either be trained anew for an individual patient or adapted from an existing model to accommodate minor anatomical differences. The training process in the PBD simulator is expected to take approximately six hours.
- Given the desired target configuration, the proposed C-GAIL path planner gives a set of configurations to move from a starting position to the target and outputs an optimal path for the catheter.
- (optional) A patient-specific phantom is manufactured, and clinicians can teleoperate the robotic catheter to perform *in-vitro* experiments. The C-GAIL path is rendered through a Graphical User Interface (GUI), serving as path guidance for the clinicians. This enables clinicians to acquire experience prior to the actual interventions, thereby reducing the likelihood of encountering unforeseen situations.
- For *in-vivo*, *ex-vivo*, or clinical practice, the C-GAIL path is rendered through a GUI and serves as path guidance for the clinicians. The clinicians can teleoperate the robotic catheter to reach the clinical target site by following the C-GAIL path.

IV. EXPERIMENTAL SETUP

The proposed workflow for the simulation and *in-vitro* user study is illustrated in Fig. 4. Firstly, a 3D mesh model is reconstructed from the CTA images of a specific patient, and a deformable environment is built using the PBD approach [43]. Then, the proposed C-GAIL network is trained using demonstrations provided by experts, which outputs an optimal path for the catheter. The C-GAIL network utilizes expert demonstrations to learn and transfer expert experience, which can provide path references for non-expert users and even autonomous catheters.

In addition to evaluating the path planning algorithm based on C-GAIL, this paper also includes control experiments (path following experiments) to verify the feasibility of executing the planned path. The *in-vitro* experiments used human-in-the-loop teleoperation control to guide the catheter along the planned path. It is worth noting that while control strategies are not the focus of this paper, they were merely included in the experiments to evaluate the feasibility and performance of the path planner. Teleoperation is more commonly used and easier to implement in practice, making it the method of choice for the *in-vitro* experiments. It is important to note that any control algorithm could theoretically be used to execute the path planned in this paper.

A. In-Silico Path Planning Setup

1) Hardware Specification: Experiments are carried out on a computer equipped with an Intel(R) Core(TM) i9-9900KF CPU @3.60 GHz 3.60 GHz processor and 32.0 GB RAM, with an NVIDIA GeForce RTX2080Ti GPU card.

2) Experimental Protocol: The purpose of the *in-silico* experiments is to validate that, given the curvature constraints of the robotic catheter, the paths obtained by the proposed C-GAIL network have better performance than the state-of-the-art GAIL approach in a static environment and are also capable to operate in a complex dynamic environment.

Training and testing were conducted in a single aortic model. For the training, 70 demonstrations were recorded using a joystick by one expert user, who performed catheter navigation through vessels in the aortic model for a PCI. The "expert user" mentioned pertains to an individual proficient with both joystick operation and this specific simulator. Future research endeavors will focus on training cardiologists, who possess at least five years of endovascular procedure experience, in the operation of this simulator system. Subsequently, we plan to collect their demonstrations to further enrich our study. The number of experiments for comparison was set to 100. Different start configurations in the descending aorta and possible target positions were chosen to make the training more generally valid. There are three possible start configurations distributed within 5.3 cm along the descending aorta. There are five target positions distributed in a spherical space with a radius of 3 cm near the coronaries and the vessel walls. Furthermore, the target moves in response to vessel deformations, which are triggered by the catheter's contact and the periodic motion of the heartbeat. The introduction of variability into the simulation model enriches the training data with diverse configurations. While such

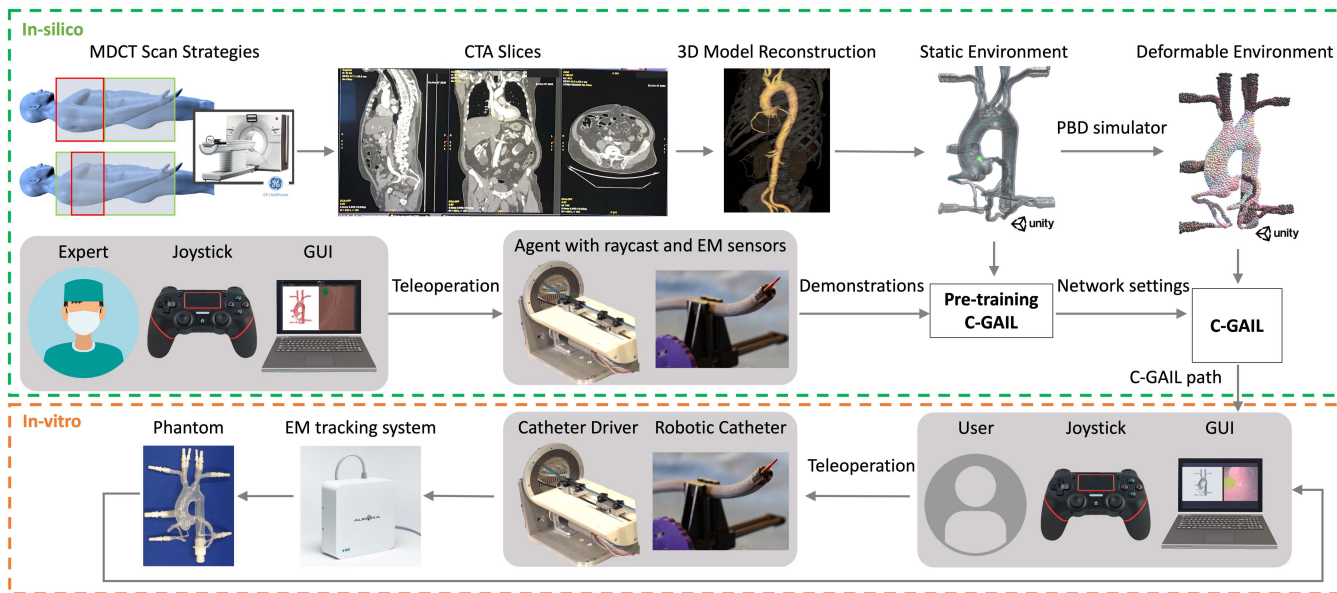


Fig. 4. Workflow for simulation and *in-vitro* user study. First, a 3D model is reconstructed from CTA images for a specific patient, and a deformable environment is built. Next, based on expert demonstrations, the C-GAIL network is trained to provide an optimal path. This path is then rendered through a GUI for the *in-vitro* experiments and serves as path guidance for users.

TABLE III
TRAINING PARAMETERS FOR C-GAIL AND GAIL

Parameter	Value	Parameter	Value
PPO beta	5.0e-4	PPO gamma	0.99
max steps	5.0e5	GAIL gamma	0.99
batch size	1024	buffer size	10240

All parameters are defined in the Unity ML-Agents Toolkit [52].

variability may initially impede convergence, it has the potential to significantly improve the network model's robustness and generalizability, as discussed in [50]. The robustness will be assessed through performance metrics, to be detailed in Section IV-C, with a particular focus on success rate and targeting error.

The C-GAIL network training was carried out in two phases: pre-training in a rigid, computationally less heavy environment, where the tuning of the network parameter settings is performed; re-training in a deformable environment, starting with the previously tuned network settings. Pre-training helps reduce the time required to obtain network settings with empirical parameters and compare the differences in agent behavior under different settings. The training parameters for the C-GAIL is presented in Table III.

The work from Chi et al. [10] is used as a reference to compare with. It's important to note that we do not directly adopt the parameters from Chi et al.'s work, as we are addressing different robotic platforms. Instead, to keep consistency in comparison, we set the same training parameters for the state-of-the-art GAIL and our proposed C-GAIL. The GAIL network architecture of [10] is adopted with minor modifications: each layer has 64 units and a Swish activation function [51]. The GAIL network undergoes training with an additional set of 70 demonstrations,

recorded by the same expert user and within the same simulation environment as utilized for the C-GAIL training process. The prior studies by Chi et al. [30], [31] introduced an LfD method based on Dynamical Movement Primitives (DMPs) and Gaussian Mixture Models (GMMs). Later, they improved the RL part by including model-free GAIL loss. Therefore, their GAIL network model was selected for comparison in our study. Other methodologies applied in deformable environments, as summarized in Table I, are primarily designed for passive, non-steerable instruments. The wall-following technique described in [20] is not apt for navigating through vessels with multiple branches. The hybrid A* approach [19] seeks the optimal path in a 2D plane, whereas the true 3D optimal path is determined using RRT*. However, RRT* may not be ideal in tightly narrow and tortuous vessels due to its potential to produce sub-optimal paths that run dangerously close to vessel walls.

B. In-Vitro Validation Setup

1) **Hardware Specification:** The *in-vitro* experimental setup, including the following devices, is depicted in Fig. 5.

a) **Phantom:** Experiments were performed in a transparent, deformable silicone aortic phantom (T-S-N-002, Elastrat Sarl, Geneva, Switzerland).

b) **Robotic catheter:** The custom-made robotic catheter is fabricated out of Nitinol using metal laser cutting technology and is actuated by four integrated Pneumatic Artificial Muscles (PAMs) [53], [54]. The outer diameter of the catheter is 7 mm, and the length is 900 mm. The distal Nitinol segment is 75 mm long and includes a 50 mm long steerable distal segment. This steerable distal segment has 2-Degree of Freedom (DoF) bending motion by concurrently controlling two antagonistic pairs of the PAMs. The maximum bending angle is 90°.

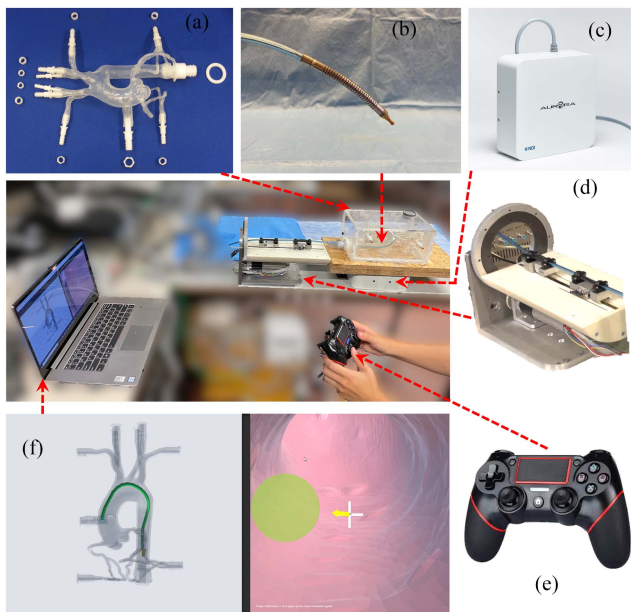


Fig. 5. *In-vitro* experimental setup to validate the proposed path planning approach: (a) Silicone aortic phantom; (b) robotic catheter; (c) Aurora EM field generator; (d) sleeve-based catheter driver; (e) wireless controller; (f) the GUI as visual feedback.

c) Electromagnetic field generator: An Electromagnetic (EM) field generator (Northern Digital Inc., Waterloo, Canada) is placed beneath the phantom. A 6-DoF EM sensor (Northern Digital Inc., Waterloo, Canada) is embedded at the tip of the catheter to track its pose.

d) Catheter driver: The robotic catheter driver system is described in [55]. The sleeve-based catheter driver has two pneumatically actuated grippers that grasp the catheter alternately and insert the catheter in a relay fashion. The maximum insertion (and retraction) speed is set as 5mm/s.

e) Joystick: The teleoperated catheter insertion and bending are realized through velocity control of the catheter driver and pressure control of the PAMs, respectively, using a wireless controller (Yues, Dublin, Ireland).

f) GUI: The path planning is visualized by a GUI, which includes an external projected view showing the aorta, path, and pose of the catheter tip, and an internal view showing the next waypoint and suggested bend direction. Guided by the internal view, users are advised on the optimal direction and degree of bend needed from the catheter tip's current position to achieve precise positioning.

2) Experimental Protocol: The objective of the *in-vitro* experiments is to validate whether the path obtained from the proposed C-GAIL path planner is more compatible with the actual steering capability of the catheter. Therefore, it can also be verified whether this path can better help the user steer the catheter accurately to the target.

For the *in-vitro* comparison with C-GAIL, we chose the traditional centerline-following approach. The centerline path is widely used in interventions [56], [57], whereas GAIL approach

(which was served as a comparison in the *in-silico* experiments) has not yet been validated in clinical practice. Moreover, both GAIL and C-GAIL are RL approaches, which have limited interpretability. Therefore, it may be suggested to use traditional approaches in parallel with learning-based approaches in order to provide a more transparent and explainable analysis. By comparing C-GAIL with the traditional centerline approach, a more interpretable comparison can be achieved.

User-involved control experiments were carried out. A single participant with an engineering background and prior experience with robotic catheters was involved. This individual had not participated in the *in-silico* experiments and was distinct from the expert user who provided the demonstrations for network training. In each trial, the user teleoperates with the robotic catheter, tries to pass through each waypoint, and finally reaches the target. During experiments, the user is instructed not to directly observe the transparent phantom. The user is instead required to rely on visual feedback provided by the GUI displayed on a conventional 2D monitor for his (her) teleoperation actions. The GUI provides critical feedback to users. It displays the catheter's tip pose, captured through EM tracking. By visualizing this alongside the rendered phantom, users can effectively gauge their proximity to the vessel walls. This feature is instrumental in preventing collisions or applying excessive force against the vessels. The maximum operation time is set to 3 minutes. If the maximum operation time is exceeded and the target is still not reached, the experiment will be forcibly stopped and be regarded as a failure. Setting this stopping criterion can avoid the following two cases: 1) The user rushes to finish the experiment without considering the performance; 2) The user tries excessively to get better performance while the procedure is very time-consuming.

The user's performance was compared in two scenarios: with the C-GAIL assistance and centerline assistance. The waypoints from $C_{centerline}$ were utilized in the centerline-following approach. The C-GAIL network was trained using different targets and obtained a path to reach an unseen target (that was not used during training). To largely eliminate the impact of the user's learning curve, the user is required to be pre-trained. Only when the learning curve converges to a plateau can we assume that the user has stable catheter manipulation abilities. The user pre-training experiments are repeated ten times. After that, control experiments with the same C-GAIL path are conducted ten times. Similarly, the pre-training experiments with the centerline and the control experiments with the same centerline are repeated ten times each. The experiments with the C-GAIL path are first performed to eliminate experience learned from the other scenario.

C. Performance Metrics

To evaluate clinical performance during endovascular procedures, clinicians typically utilize a range of benchmarks, such as patient outcomes, procedural success, and safety measures [58]. Engineering studies [59], [60] have focused on objectively determining cardiologists' proficiency through catheter kinematics

analysis. Building upon these established evaluation approaches, our research integrates specific performance metrics to thoroughly quantify the performance of *in-silico* and *in-vitro* experimental results. The statistically significant difference between the proposed method and others is evaluated via the Kruskal-Wallis test in this work, with a significance level of 0.05.

1) Success Rate (δ): Success rate represents the percentage of successes among the total number of attempts.

$$\delta = n_s/n \quad (7)$$

where n_s is the number of successes to reach the target within a given time, and n is the number of attempts.

2) Timesteps (T_s): For *in-silico* experiments, at each time step, the agent receives observations, takes an action according to its policy and receives rewards. T_s is defined as the number of time steps moving from the start configuration to the target.

$$T_s = N_g - N_0 + 1 \quad (8)$$

where N_0 and N_g are the first and last time step, respectively.

3) Duration (T): Duration is the length of time a single experiment lasts from start to stop. An experiment stops when the target or the maximum duration has been reached.

$$T = t_g - t_0 \quad (9)$$

where t_0 and t_g are the first and last timestamp, respectively. The total duration of the procedure assumes significance not only in terms of its impact on patient safety but also in relation to patient comfort and recovery. Prolonged procedures may lead to increased patient discomfort and extended recovery periods, making duration a valuable indicator of procedure performance, particularly with regard to safety. Moreover, extended durations place a burden on hospital resources, tying up catheterization labs and medical personnel and potentially escalating operational expenses.

4) Tracking Error (T_r): Tracking error is the distance between the *in-vitro* trajectory obtained from the EM sensor and the desired path. The desired path is obtained through path planning, followed by B-spline curve fitting and resampling. This criterion is used to evaluate the path following capability.

$$T_r(t) = \|\mathbf{p}_t^d - \mathbf{p}_t\| \quad (10)$$

where \mathbf{p}_t^d is the desired position and \mathbf{p}_t is the actual position. Tracking error is employed as a safety metric, with lower tracking errors denoting a trajectory that closely matches the intended path, thereby indicating a lower likelihood of complications, including vascular damage.

5) Targeting Error (T_a): Targeting error is the minimum distance to the target along the trajectory. This criterion is used to evaluate the accuracy when reaching the target.

$$T_a = \min \|\mathbf{q}_g - \mathbf{p}_t\| \quad (11)$$

Targeting error is utilized as an indicator of procedural technical success, where reduced targeting error represents precise device placement.

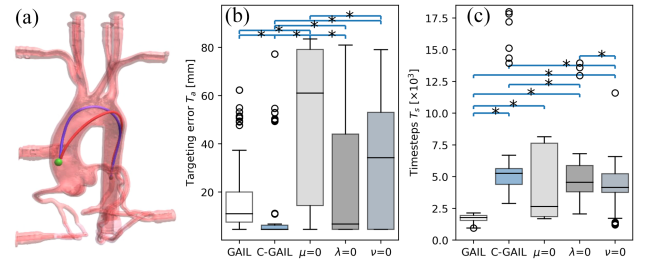


Fig. 6. *In-silico* performance comparison between the proposed C-GAIL network (purple) and the state-of-the-art GAIL network [10] (red), with respect to (a) example of trajectories, (b) targeting error T_a , and (c) timesteps T_s . An ablation study of the C-GAIL is presented when $\mu = 0$, $\lambda = 0$ or $\nu = 0$. (*, $p < 0.05$ using Kruskal-Wallis test).

V. RESULTS AND DISCUSSION

A. In-Silico Path Planning

The performance comparison of the proposed C-GAIL and the state-of-the-art GAIL [10] in a static environment is presented in Fig. 6. The number of experiments for comparison is set to 100, and results are reported regardless of whether the target was successfully reached. Fig. 6(a) shows an example of trajectories obtained by these two approaches. The C-GAIL approach generates paths with smaller targeting errors (see Fig. 6(b)). An ablation study of the C-GAIL is also presented, investigating its performance when $\mu = 0$, $\lambda = 0$, or $\nu = 0$. If we set the threshold $\epsilon = 10$, the success rate of the C-GAIL network, originally at 80%, decreases to 11%, 58%, and 48% for the scenarios when $\mu = 0$, $\lambda = 0$, and $\nu = 0$ respectively. The ablation study results, as shown in Fig. 6(b), indicate that BC, GAIL and curiosity modules are all critical for accurate target reaching. Compared to the PPO + GAIL framework utilized in neurosurgery, as detailed by Segato et al. [11], our C-GAIL network introduces further advancements by integrating both the BC and CL modules. The ablation study reveals a significant decline in performance in the absence of the BC module, i.e., when $\mu = 0$. Consequently, it is inferred that the method by Segato et al. would underperform compared to our proposed approach. Furthermore, the robustness of the proposed network is verified by the success rate of the C-GAIL network, that is 80%, compared to that of the GAIL network [10] which is only 42%, when $\epsilon = 10$. However, compared to GAIL, C-GAIL requires more timesteps to reach the target (see Fig. 6(c)). This indicates that either the path is longer or there are more samples taken along the path to achieve the same level of path length. The duration is affected by a large number of failures that often cause early termination of the experiment. A common failure is that the path planning tends to stop due to non-minor collision with the aortic arch and are therefore unsuccessful attempts. Minor collisions that cause slight deformation within reasonable stress ranges were considered harmless [61]. In our prior simulator study [43], the maximum permissible force applied by the user varies with the anatomical structure involved. For instance, in the aorta, the maximum force is capped at 0.8N. An absolute collision force is determined using Newton's Second Law of

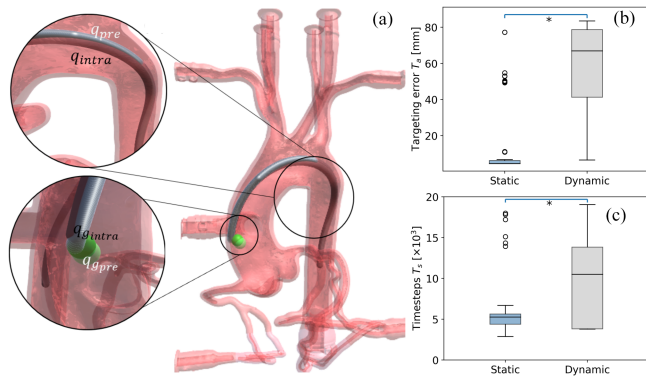


Fig. 7. *In-silico* performance of the proposed C-GAIL network in static and dynamic environments: (a) The intra-operative adaptation of the pre-operative path q_{pre} when the environment is deformable and the target moves; (b) Targeting error T_a and (c) Timesteps T_s in static and dynamic environments. (*, $p < 0.05$ using Kruskal-Wallis test).

Motion. A collision is classified as minor if the resultant force is below the maximum threshold and there is no penetration.

The agent was then trained using pre-trained weights from the static environment in a dynamic environment, where deformations are caused by contact with the catheter and the heartbeat motion. Fig. 7(a) demonstrates the ability of real-time planning in a complex dynamic environment with deformable vessels and a moving target. The top zoom-in view shows that the paths of pre-trained q_{pre} and intraoperatively trained q_{intra} are initially close and then separate in the aortic arch, where the degree of deformation is greater. The bottom zoom-in view shows the change from the initial target position q_{gpre} to the intraoperative target position q_{gintra} . Fig. 7(b) and (c) present performance comparisons in static and dynamic environments. The timesteps are much more in the deformable environment. This is due to the fact that there are more possibilities when interacting with a deformable environment than with a static one. Due to the greater complexity of navigation and low success rate, targeting error is larger and more widely distributed than in the static environment. Nevertheless, when considering only the successful trials, the targeting error is observed to be 4.76 ± 0.57 mm in the static environment and 7.57 ± 0.65 mm in the dynamic environment, respectively, demonstrating comparable results. The success rate of 17% is relatively low but indicates that it is possible to find a feasible path in a constrained environment, compared to the success rate of 0% for the GAIL network [10] in the dynamic environment. A common failure is the inability to reach the moving targets with a distance threshold of 10 mm. Including this distance threshold to reach a target in the curriculum module would improve network performance, such as success rate. This would be investigated at a later stage. The limited bending capability of robotic catheters and the presence of moving targets in deformable environments led to a reduced success rate within a limited number of timesteps. Despite the relatively low success rate of C-GAIL, it has outperformed the state-of-the-art approach.

One limitation of our proposed method, particularly in medical applications, is the exclusion of blood fluid flow dynamics in

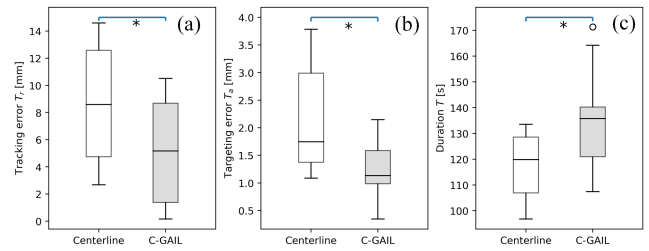


Fig. 8. *In-vitro* performance comparison between C-GAIL path and centerline, with respect to (a) tracking error T_r , (b) targeting error T_a , and (c) duration T . (*, $p < 0.05$ using Kruskal-Wallis test).

our developed simulator. To address this, future iterations should incorporate fluid dynamics, potentially using subject-specific geometries as suggested in [62], [63]. The presence of blood introduces friction and resistance against the catheter as it moves through the vessels [64]. Integrating fluid dynamics could yield more precise predictions of vessel deformation and catheter movement. Such enhancements are likely to elevate the realism of the simulated scenarios, thereby improving the accuracy of the path planning to better reflect real-world conditions.

B. In-Vitro Validation

To essentially eliminate the impact of the user's learning curve, the user is required to be pre-trained. For example, the learning curve of the targeting error by following the C-GAIL path decreased from 3.6 to ~ 2 mm in ten trials. The user can achieve a targeting error of 0.23 mm in the later stage. Since the learning curve converges to a plateau, it can be concluded that the user has stable catheter manipulation ability. A video is made available showing example experiments of following the C-GAIL path and the centerline¹.

The performance comparison between the C-GAIL path and the centerline is shown in Fig. 8. The C-GAIL path leads to a smaller tracking error of 5.18 ± 3.48 mm. It confirms that C-GAIL leads to a path that can be followed better by the robotic catheter. Furthermore, the C-GAIL path also shows a smaller targeting error of 1.26 ± 0.55 mm (Fig. 8(b)). Clinicians typically indicate an accuracy range of 1–3 mm as acceptable [65], [66]. Therefore, the mean targeting error of 1.26 mm effectively meets these clinical accuracy requirements. Following the C-GAIL path takes a longer time than following the centerline. This is interpretable given that since the user learned that the centerline waypoints could not be reached anyway when passing the aortic arch, the user kept inserting the catheter at the maximum bending angle and spent less effort following the centerline. While in the other scenario, the user realized that (s)he could follow the C-GAIL path waypoints. Therefore, it takes a longer time than following the centerline. Two of the ten experiments with the C-GAIL path took longer because the user made a retraction motion in order to re-reach the target more accurately. Both the C-GAIL path and centerline following experiments had a 100% success rate. To reduce tracking and targeting errors, future

¹https://youtu.be/GhBi_xHTMFw

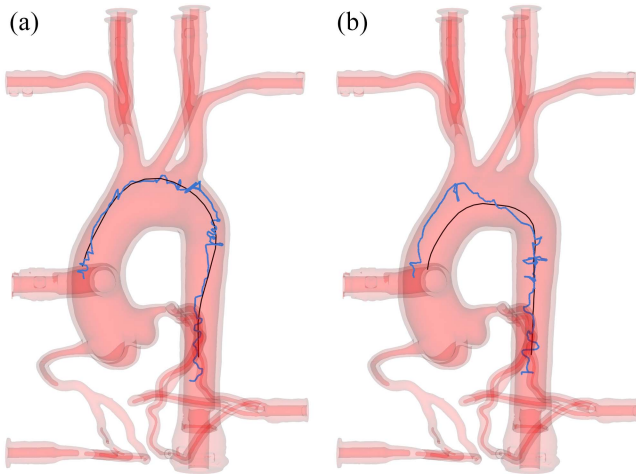


Fig. 9. Representative *in-vitro* trajectories (blue) and path guidance (black) using: (a) C-GAIL path, and (b) centerline.

efforts could explore the use of control input devices offering a broader range of motion than joysticks, such as haptic devices.

Fig. 9 presents a representative graphical comparison of actual trajectories and path guidance in two scenarios: following the C-GAIL path and following the centerline. The trajectories of the catheter tip following the C-GAIL path are more stable and smoother, with a curvature of $3.1 \pm 26.6 \text{ mm}^{-1}$, compared to a curvature of $3.5 \pm 38.9 \text{ mm}^{-1}$ when following the centerline. In the other scenario, the catheter tip can follow the centerline well at the beginning. However, the trajectory then moves away from the centerline as the catheter passes through the aortic arch due to the limited bending capability. It is important to clarify that the trajectory refers to the movement of the catheter tip. In the *in-vitro* environment, where gravity plays a role, contact between the catheter body and the vessel walls is unavoidable. However, such contact poses minimal risk due to the catheter body's non-sharp nature. The focus of this study does not extend to the catheter's back-end configuration, which may be pertinent for advancing to higher levels of autonomy, such as achieving autonomous navigation along the vessels [40]. For this objective, capturing the entire catheter's shape using Fiber Bragg Grating (FBG) could prove beneficial.

In this research, the robotic catheter operation was facilitated through teleoperation. The control technique does not influence the path planning phase because the catheter's constraints, including its bending capabilities, have been preemptively incorporated. Additionally, this dimension was further investigated in a subsequent study [67], wherein 15 participants with diverse experience levels evaluated the system's effectiveness using C-GAIL path planning within various modes of interaction.

C. Transferability

To further generalize the proposed path planning framework, *in-silico* experiments were conducted in a different aortic anatomy (Materialise NV, Leuven, Belgium). 70 demonstrations were recorded, and 100 testing trials were performed. The

TABLE IV
IN-SILICO PERFORMANCE OF THE PROPOSED C-GAIL NETWORK IN A DIFFERENT AORTIC ANATOMY

T_a (mm)					T_s ($\times 10^3$)					δ
25th	median	75th	mean	std	25th	median	75th	mean	std	(%)
6.58	6.84	8.57	17.98	23.51	9.41	10.22	11.59	9.71	2.78	79

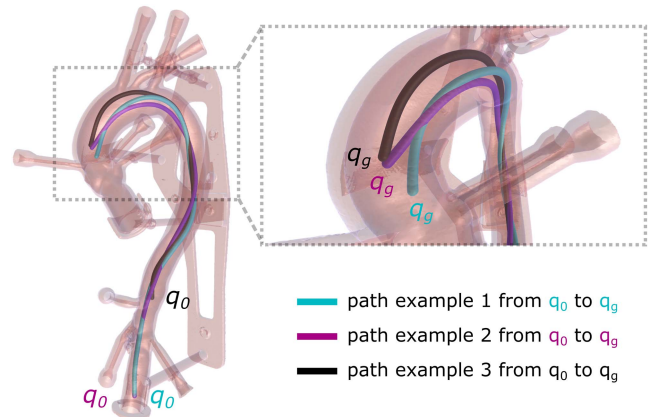


Fig. 10. Examples of *in-silico* C-GAIL paths in a different aortic anatomy (Materialise NV, Leuven, Belgium).

success rate of the proposed C-GAIL network was 79% when $\epsilon = 10$. Other performance values with respect to targeting error and timesteps are summarized in Table IV. Representative paths obtained by the C-GAIL approach are shown in Fig. 10. These results indicate the robustness and feasibility of applying the proposed path planning framework in anatomies with different geometries.

This paper employs an EM sensor to measure the tip pose, which has been validated in a phantom study. EM sensor has demonstrated its efficacy also in *in-vivo* environments [68], [69] considering its small size ($< 1 \text{ mm}$ in diameter and $< 10 \text{ mm}$ in length) and bio-compatibility. Furthermore, other sensors, such as FBG sensor, as well as imaging modalities, can also be utilized to obtain the catheter tip pose and the body shape. In certain specific cases (e.g., free space), the catheter tip pose can also be obtained with a sensorless approach, e.g., an accurate forward kinematic model if control variables are provided [54]. One limitation of this study is that there was no intra-operative environment reconstruction for the *in-vitro* experiments. Instead, a simulated deformable model was utilized to predict intra-operative deformations. In clinical settings, real-time vessel reconstruction from IntraVascular UltraSound (IVUS) or Optical Coherence Tomography (OCT) images would be suitable for providing raycast observations elaborated in this work.

VI. CONCLUSION

This study set out to design a robust path planning approach respecting the kinematics of robotic catheters and real-time changes in deformable cluttered environments. This path planning approach uniquely accounts for both the deformable nature

of the environment and the dynamic movements of the target, distinguishing it from existing methods. *In-vitro* experiments and an extensive follow-up user study [67] underscore the algorithm's feasibility in generating suitable paths that align with the actual steering capability of the catheter and the deformable environment, thereby enhancing navigation support with greater accuracy.

The insights gained from this study add to the rapidly expanding field of autonomous navigation for robotic catheters. The findings of this study suggest that the proposed path planner can effectively handle the uncertainty present in vessel deformation.

A limitation of our study is the absence of intra-operative environment reconstruction during the *in-vitro* experiments. In clinical practice, real-time reconstruction of vessels using IVUS or OCT images would be advantageous for generating the raycast observations discussed herein. Further clinical studies that involve real-time vessel reconstruction will be carried out. Additionally, future efforts could benefit from integrating blood fluid flow dynamics into the simulator, thereby increasing the realism of simulated scenarios and enhancing path planning accuracy.

REFERENCES

- [1] A. P. Durko et al., "Annual number of candidates for transcatheter aortic valve implantation per country: Current estimates and future projections," *Eur. Heart J.*, vol. 39, no. 28, pp. 2635–2642, 2018.
- [2] R. Aggarwal et al., "Virtual reality simulation training can improve inexperienced surgeons' endovascular skills," *Eur. J. Vasc. Endovascular Surg.*, vol. 31, no. 6, pp. 588–593, 2006.
- [3] C. Culmone et al., "Follow-the-leader mechanisms in medical devices: A review on scientific and patent literature," *IEEE Rev. Biomed. Eng.*, vol. 16, pp. 439–455, 2023.
- [4] T. da Veiga et al., "Challenges of continuum robots in clinical context: A review," *Prog. Biomed. Eng.*, vol. 2, no. 3, 2020, Art. no. 032003.
- [5] A. Ali et al., "First expert evaluation of a new steerable catheter in an isolated beating heart," *Cardiovasc. Eng. Technol.*, vol. 11, no. 6, pp. 769–782, 2020.
- [6] N. Nayar, S. Jeong, and J. P. Desai, "Design and control of 5-DoF robotically steerable catheter for the delivery of the mitral valve implant," in *Proc. IEEE Int. Conf. Robot. Automat.*, 2021, pp. 12268–12274.
- [7] M. H. D. Ansari et al., "Proof-of-concept medical robotic platform for endovascular catheterization," in *Proc. Conf. New Technol. Comput. Robot. Assist. Surg.*, 2022.
- [8] G. Borghesan et al., "ATLAS: Autonomous intraluminal surgery: System specifications for targeted intraluminal interventions," 2020. [Online]. Available: https://atlas-itn.eu/d102_main/
- [9] A. Favaro et al., "An evolutionary-optimized surgical path planner for a programmable bevel-tip needle," *IEEE Trans. Robot.*, vol. 37, no. 4, pp. 1039–1050, Aug. 2021.
- [10] W. Chi et al., "Collaborative robot-assisted endovascular catheterization with generative adversarial imitation learning," in *Proc. IEEE Int. Conf. Robot. Automat.*, 2020, pp. 2414–2420.
- [11] A. Segato et al., "Inverse reinforcement learning intra-operative path planning for steerable needle," *IEEE Trans. Biomed. Eng.*, vol. 69, no. 6, pp. 1995–2005, Jun. 2022.
- [12] J. Wang et al., "Intravascular catheter navigation using path planning and virtual visual feedback for oral cancer treatment," *Int. J. Med. Robot. Comput. Assist. Surg.*, vol. 7, no. 2, pp. 214–224, 2011.
- [13] J.-Q. Zheng et al., "Towards 3D path planning from a single 2D fluoroscopic image for robot assisted fenestrated endovascular aortic repair," in *Proc. IEEE Int. Conf. Robot. Automat.*, 2019, pp. 8747–8753.
- [14] D. Huang et al., "An interactive 3D preoperative planning and training system for minimally invasive vascular surgery," in *Proc. IEEE 12th Int. Conf. Comput. Aided Des. Comput. Graph.*, 2011, pp. 443–449.
- [15] H. Qian et al., "Towards rebuild the interventionist's intra-operative natural behavior: A fully sensorized endovascular robotic system design," in *Proc. IEEE Int. Conf. Med. Imag. Phys. Eng.*, 2019, pp. 1–7.
- [16] Y. Cho et al., "Image processing based autonomous guidewire navigation in percutaneous coronary intervention," in *Proc. IEEE Int. Conf. Consum. Electron. Asia*, 2021, pp. 1–6.
- [17] P. Schegg et al., "Automated planning for robotic guidewire navigation in the coronary arteries," in *Proc. IEEE 5th Int. Conf. Soft Robot.*, 2022, pp. 239–246.
- [18] S. R. Ravigopal, T. A. Brumfiel, and J. P. Desai, "Automated motion control of the COAST robotic guidewire under fluoroscopic guidance," in *Proc. IEEE Int. Symp. Med. Robot.*, 2021, pp. 1–7.
- [19] S. R. Ravigopal et al., "Fluoroscopic image-based 3-D environment reconstruction and automated path planning for a robotically steerable guidewire," *IEEE Robot. Automat. Lett.*, vol. 7, no. 4, pp. 11918–11925, Oct. 2022.
- [20] G. Fagogenis et al., "Autonomous robotic intracardiac catheter navigation using haptic vision," *Sci. Robot.*, vol. 4, no. 29, 2019, Art. no. eaaw1977.
- [21] J. Fauser et al., "Generalized trajectory planning for nonlinear interventions," in *Proc. Int. Workshop Comput. Assist. Robot. Endoscopy*, 2018, pp. 46–53.
- [22] J. Fauser et al., "Planning for flexible surgical robots via Bézier spline translation," *IEEE Robot. Automat. Lett.*, vol. 4, no. 4, pp. 3270–3277, Oct. 2019.
- [23] J. Fauser et al., "Optimizing clearance of Bézier spline trajectories for minimally-invasive surgery," in *Proc. Int. Conf. Med. Imag. Comput. Imag. Assist. Interv.*, 2019, pp. 20–28.
- [24] J. Guo, Y. Sun, and S. Guo, "A training system for vascular interventional surgeons based on local path planning," in *Proc. IEEE Int. Conf. Mechatron. Automat.*, 2021, pp. 1328–1333.
- [25] M. Gao et al., "Three-dimensional path planning and guidance of leg vascular based on improved ant colony algorithm in augmented reality," *J. Med. Syst.*, vol. 39, no. 11, 2015, Art. no. 133.
- [26] F. Qi et al., "Kinematic analysis and navigation method of a cable-driven continuum robot used for minimally invasive surgery," *Int. J. Med. Robot. Comput. Assist. Surg.*, vol. 15, no. 4, 2019, Art. no. e2007.
- [27] Z. Li et al., "Path planning for endovascular catheterization under curvature constraints via two-phase searching approach," *Int. J. Comput. Assist. Radiol. Surg.*, vol. 16, no. 4, pp. 619–627, 2021.
- [28] H. Rafii-Tari et al., "Learning-based modeling of endovascular navigation for collaborative robotic catheterization," in *Proc. Int. Conf. Med. Image Comput. Comput.-Assist. Interv.*, 2013, pp. 369–377.
- [29] H. Rafii-Tari et al., "Hierarchical HMM based learning of navigation primitives for cooperative robotic endovascular catheterization," in *Proc. Int. Conf. Med. Imag. Comput. And Comput. Assist. Interv.*, 2014, pp. 496–503.
- [30] W. Chi et al., "Trajectory optimization of robot-assisted endovascular catheterization with reinforcement learning," in *Proc. IEEE/RSJ Int. Conf. Intell. Robot. Syst.*, 2018, pp. 3875–3881.
- [31] W. Chi et al., "Learning-based endovascular navigation through the use of non-rigid registration for collaborative robotic catheterization," *Int. J. Comput. Assist. Radiol. Surg.*, vol. 13, no. 6, pp. 855–864, 2018.
- [32] Y. Zhao et al., "Surgical GAN: Towards real-time path planning for passive flexible tools in endovascular surgeries," *Neurocomputing*, vol. 500, pp. 567–580, 2022.
- [33] A. T. Tibebe et al., "Towards autonomous robotic catheter navigation using reinforcement learning," in *Proc. Joint Workshop New Technol. Comput./Robot. Assist. Surg.*, 2014, pp. 163–166.
- [34] H. You et al., "Automatic control of cardiac ablation catheter with deep reinforcement learning method," *J. Mech. Sci. Technol.*, vol. 33, no. 11, pp. 5415–5423, 2019.
- [35] T. Behr et al., "Deep reinforcement learning for the navigation of neurovascular catheters," *Curr. Directions Biomed. Eng.*, vol. 5, no. 1, pp. 5–8, 2019.
- [36] L. Karstensen et al., "Autonomous guidewire navigation in a two dimensional vascular phantom," *Curr. Directions Biomed. Eng.*, vol. 6, no. 1, 2020, Art. no. 20200007.
- [37] J. Kweon et al., "Deep reinforcement learning for guidewire navigation in coronary artery phantom," *IEEE Access*, vol. 9, pp. 166409–166422, 2021.
- [38] F. Meng et al., "Evaluation of a reinforcement learning algorithm for vascular intervention surgery," in *Proc. IEEE Int. Conf. Mechatron. Automat.*, 2021, pp. 1033–1037.
- [39] L. Karstensen et al., "Learning-based autonomous vascular guidewire navigation without human demonstration in the venous system of a porcine liver," *Int. J. Comput. Assist. Radiol. Surg.*, vol. 17, pp. 2033–2040, 2022.
- [40] A. Pore et al., "Autonomous navigation for robot-assisted intraluminal and endovascular procedures: A systematic review," *IEEE Trans. Robot.*, vol. 39, no. 4, pp. 2529–2548, Aug. 2023.

- [41] D. Wu et al., "A review on machine learning in flexible surgical and interventional robots: Where we are and where we are going," *Biomed. Signal Process. Control*, vol. 93, 2024, Art. no. 106179.
- [42] A. Pore et al., "Learning from demonstrations for autonomous soft-tissue retraction," in *Proc. IEEE Int. Symp. Med. Robot.*, 2021, pp. 1–7.
- [43] Z. Li et al., "Position-based dynamics simulator of vessel deformations for path planning in robotic endovascular catheterization," *Med. Eng. Phys.*, vol. 110, 2022, Art. no. 103920.
- [44] Z. Li et al., "Simulation of deformable vasculature for robot-assisted endovascular catheterization," in *Proc. Conf. Int. Soc. Med. Innov. Technol.*, 2022, pp. 1–2.
- [45] D. Pathak et al., "Curiosity-driven exploration by self-supervised prediction," in *Proc. Int. Conf. Mach. Learn.*, 2017, pp. 2778–2787.
- [46] S. Narvekar et al., "Source task creation for curriculum learning," in *Proc. Int. Conf. Auton. Agents Multiagent Syst.*, 2016, pp. 566–574.
- [47] J. Schulman et al., "Proximal policy optimization algorithms," 2017, *arXiv:1707.06347*.
- [48] J. Ho et al., "Generative adversarial imitation learning," in *Proc. Adv. Neural Inf. Process. Syst.*, vol. 29, 2016, pp. 4572–4580.
- [49] F. Torabi et al., "Behavioral cloning from observation," in *Proc. 27th Int. Joint Conf. Artif. Intell.*, 2018, pp. 4950–4957.
- [50] W. Xiao et al., "Multigoal visual navigation with collision avoidance via deep reinforcement learning," *IEEE Trans. Instrum. Meas.*, vol. 71, 2022, Art. no. 2505809.
- [51] P. Ramachandran et al., "Searching for activation functions," 2017, *arXiv:1710.05941*.
- [52] A. Juliani et al., "Unity: A general platform for intelligent agents," 2018, *arXiv:1809.02627*.
- [53] A. Devreker et al., "Fluidic actuation for intra-operative in situ imaging," in *2015 IEEE/RSJ Int. Conf. Intell. Robots Syst.*, 2015, pp. 1415–1421.
- [54] D. Wu et al., "Hysteresis modeling of robotic catheters based on long short-term memory network for improved environment reconstruction," *IEEE Robot. Automat. Lett.*, vol. 6, no. 2, pp. 2106–2113, Apr. 2021.
- [55] O. Al-Ahmad et al., "Force control with a novel robotic catheterization system based on braided sleeve grippers," *IEEE Trans. Med. Robot. Bionics*, vol. 5, no. 3, pp. 602–613, Aug. 2023.
- [56] J. P. Sobocinski et al., "The benefits of EVAR planning using a 3D workstation," *Eur. J. Vasc. Endovascular Surg.*, vol. 46, no. 4, pp. 418–423, 2013.
- [57] S. Ramcharitar et al., "Technology insight: Magnetic navigation in coronary interventions," *Nature Clin. Pract. Cardiovasc. Med.*, vol. 5, no. 3, pp. 148–156, 2008.
- [58] E. C. Saricilar et al., "Evaluation of tools to assess operative competence in endovascular procedures: A systematic review," *ANZ J. Surg.*, vol. 91, no. 9, pp. 1682–1695, 2021.
- [59] C. Duran et al., "Kinematics effectively delineate accomplished users of endovascular robotics with a physical training model," *J. Vasc. Surg.*, vol. 61, no. 2, pp. 535–541, 2015.
- [60] E. B. Mazomenos et al., "Catheter manipulation analysis for objective performance and technical skills assessment in transcatheter aortic valve implantation," *Int. J. Comput. Assist. Radiol. Surg.*, vol. 11, pp. 1121–1131, 2016.
- [61] X. Ye et al., "A fast and stable vascular deformation scheme for interventional surgery training system," *Biomed. Eng. Online*, vol. 15, no. 1, pp. 1–14, 2016.
- [62] E. L. Schwarz et al., "Beyond CFD: Emerging methodologies for predictive simulation in cardiovascular health and disease," *Biophys. Rev.*, vol. 4, no. 1, 2023, Art. no. 011301.
- [63] T. Jianu et al., "Autonomous catheterization with open-source simulator and expert trajectory," 2024, *arXiv:2401.09059*.
- [64] R. M. Wagner et al., "Bio-tribology of vascular devices: A review of tissue/device friction research," *Biotribology*, vol. 25, 2021, Art. no. 100169.
- [65] H. Nijland et al., "Evaluation of accuracy and precision of CT-guidance in radiofrequency ablation for osteoid osteoma in 86 patients," *PLoS One*, vol. 12, no. 4, 2017, Art. no. e0169171.
- [66] F. Bourier et al., "Sensor-based electromagnetic navigation (mediguide): How accurate is it? A phantom model study," *J. Cardiovasc. Electrophysiol.*, vol. 26, no. 10, pp. 1140–1145, 2015.
- [67] D. Wu et al., "Comparative analysis of interactive modalities for intuitive endovascular interventions," *IEEE Trans. Vis. Comput. Graph.*, early access, Feb. 06, 2024, doi: [10.1109/TVCG.2024.3362628](https://doi.org/10.1109/TVCG.2024.3362628).
- [68] M. Ourak et al., "Fusion of biplane fluoroscopy with fiber Bragg grating for 3D catheter shape reconstruction," *IEEE Robot. Automat. Lett.*, vol. 6, no. 4, pp. 6505–6512, Oct. 2021.
- [69] X. T. Ha et al., "Robust catheter tracking by fusing electromagnetic tracking, fiber Bragg grating and sparse fluoroscopic images," *IEEE Sensors J.*, vol. 21, no. 20, pp. 23422–23434, Oct. 2021.

Open Access provided by 'Politecnico di Milano' within the CRUI CARE Agreement